First Results of the Ground Layer Adaptive Optics System ARGOS

G. Orban de Xivry[a], S. Rabien[a], L. Busoni[b], W. Gaessler[c], M. Bonaglia[b], J. Borelli[c], M. Deysenroth[a], S. Esposito[b], H. Gemperlein[a], M. Kulas[c], M. Lefebvre[d], T. Mazzoni[b], D. Peter[c], A. Puglisi[b], W. Raab[e], G. Rahmer[d], A. Sivitilli[c], J. Storm[f], and J. Ziegleder[a]

[a]Max Planck Institut für extraterrestrische Physik, Giessenbachstrasse 1, 85748 Garching, Germany
[b]INAF Osservatorio Astrofisico di Arcetri, L.go E. Fermi 5, 50125 Firenze, Italy
[c]Max-Planck-Institut für Astronomie, Koenigstuhl 17, 69117 Heidelberg, Germany
[d]Large Binocular Observatory, North Cherry Avenue 933, Tucson, 85721 Arizona, USA
[e]European Space Agency, ESTEC, Keplerlaan 1, 2201AZ Noordwijk, The Netherlands
[f]Leibniz-Institut für Astrophysik Potsdam, An der Sternwarte 16, 14482 Potsdam, Germany

ABSTRACT

We present the first results of ARGOS, the multiple laser guide star and wavefront sensing facility for the Large Binocular Telescope. This system will deliver an improvement by a factor of two in FWHM over the $4' \times 4'$ field of view of both LUCI instruments. LUCI 1 and LUCI 2 are two near-infrared wide field imagers and multi-object spectrographs which capability and efficiency will be boosted by the increased resolution and encircled energy.

The first on-sky ground-layer adaptive optics (GLAO) loop closure with ARGOS has been achieved in Fall 2014 on the right eye of the telescope. Stable operations in closed-loop have been demonstrated in May 2015 with hour-long integration and repeated good performances over several nights. Since then, the commissioning has been proceeding with the installation of the left system and the beginning of the left on-sky operations in this Fall 2015. The next achievements will be to strengthen the operational aspects and to perform science demonstration in both imaging and spectroscopic modes. We first present the current status of the project and review the operational aspects. Then, we analyze the first combined LUCI and ARGOS observations and discuss the performances and the gains provided by ARGOS in term of scientific capabilities.

Keywords: Ground-Layer Adaptive Optics; Laser Guide Stars; Large Binocular Telescope

1. INTRODUCTION

GLAO systems are motivated by the recognition that in most astronomical sites the ground-layer and the dome turbulences are the major contributors to the total wavefront perturbation.[1–3] This is even more relevant for the Extremely Large Telescopes with their particularly large domes that increase local seeing effects.

By measuring the ground layer turbulence and using a single deformable mirror, GLAO offers a wide field correction but does not reach the diffraction limit. In addition, with the help of laser guide stars (LGS), it also provides nearly full-sky coverage because of the modest requirements on tip-tilt correction. This compromise between partial correction and large field of view (FoV) is in fact advantageous in most astronomical applications, benifiting of : the increased point source sensitivity, the increased slit coupling efficiency for spectroscopy, the reduced crowding noise in dense fields, and obviously the improved spatial resolution.

The Large Binocular Telescope (LBT) is currently the only 8-m class telescope implementing such GLAO correction : the laser guided ground layer adaptive optics system ARGOS. The telescope is equipped with two 8.4m primary mirrors, as well as adaptive secondary mirrors for the atmospheric correction and a large suite of instruments for imaging and spectroscopy from mid-infrared to visible wavelengths. Amongst those the two

Further author information: (Send correspondence to G. Orban de Xivry)
G. Orban de Xivry: E-mail: xivry@mpe.mpg.de, Telephone: (0049)089-30000-3623

LUCI[4] instruments offer imaging and multi-object spectroscopy in the near-infrared over a $4'\times4'$ field of view. In this context, the scientific motivation for the installation of a laser guide star adaptive optics system is clear : performing a ground-layer correction to strongly increase the scientific capabilities of the LUCI instruments.

The GLAO image enhancement brought by ARGOS will be beneficial for science at both low and high redshifts, covering topics as varied as stellar population in star clusters, star formation in nearby galaxies, and high redshift galaxy studies. As those distant galaxies are typically of order $0.3''$ to $0.6''$, they can directly benefit from the trade-off between spatial resolution and signal-to-noise ratio. In some cases, ARGOS could even allow to spatially resolve the velocity curves along the slit length in order to better understand the dynamics and the formation history of those primordial galaxies. Such possible observations also set strong requirements on robustness and stability of the correction in order to be able to perform the long integrations needed with good atmospheric correction and stable slit coupling.

To fullfill its objectives and improve by a factor of two in FWHM size over the $4'\times4'$ FoV, ARGOS features three pulsed Rayleigh beacons per each side of the LBT. The backscattered photons are detected by Shack-Hartmann based wavefront sensors. Those sensors includes the acquisition and stabilization of the laser spots, the gating of the required guide star height with Pockels cells and the imaging of all three Shack-Hartmann pupils on a single large frame CCD. Those measurements then feed our wavefront sensor real-time computer which is interfaced to the adaptive secondary mirror computers. In addition, the system is composed of : a quad-cell based on Avalanche Photo-Diodes (APD) tip-tilt sensor to allow the faintest tip-tilt guide stars, a dedicated calibration system also used for daytime operation, and all the necessary instrument control software.

Upon its completion and demonstrated efficiency, the combination of LUCI and ARGOS will become superior to any other ground-based multi-object spectrograph and competitive to WFC3 on HST. Indeed, WFC3[5] has a $\sim 2' \times 2'$ FoV and $0.135''\times0.121''$ pixel scale from 800nm to 1700nm, while LUCI used with ARGOS provides $4'\times4'$ FoV with $0.12''\times0.12''$ pixel scale up to the K-band. In the future, the expected efficiency of NIRSPEC[6] on JWST, covering up to $5\mu m$ wavelength and allowing multi-object spectroscopy over $\sim 3' \times 3'$, will naturally surpass the LUCI and ARGOS combination. But even in this prospect, this facility will remain competitive by its comparable specifications and its easier access. On the ground, while previous demonstrators (e.g. MAD,[7] MMT[8]) or current facility (SAM[9]) have proven the GLAO concept, ARGOS is nevertheless a unique system providing a $4'$ field of view square GLAO correction on a two-8.4m telescope.

In this paper, we present the first results of the ARGOS instrument. We start in Section 2 by giving an overview of the system and discuss operational aspects as well as selected commissioning lessons. We then focus in Section 3 on the first on-sky results obtained since December 2014 which demonstrate that ARGOS has started to deliver its expected performances. We finally summarize our current status and conclude on the prospect for the ARGOS finalization.

2. FROM HARDWARE TO OPERATIONS

The system layout as well as the development of the sub-systems have been presented multiple times in proceedings (e.g., 10–13). Here, we try to focus more on a description of the operational steps needed for the ARGOS daytime or nighttime work, and discuss some selected aspects of our learning during the commissioning together with subsequent hardware and software improvements.

Laser Propagation, Acquisition, and Spot Control Propagation of class IV lasers on-sky is naturally regulated. On U.S. soil, this requires coordination and approval of the U.S. Space command and the Federal Aviation Administration (FAA). The direct consequences are the need to submit targets about one week in advance to implement a satellite avoidance mechanism in the interlock system and to organize human aircraft spotters. The last point is necessary until an automated system can be demonstrated and authorized by the FAA. To this aim, LBT is currently testing an automated detection system based on TBAD* devices.[14]

Once authorized, the three† frequency doubled Nd:YAG laser heads are firing synchronously a ∼40ns wide pulse at 532nm at an average power of 18W each. After the appropriate beam shaping, the light falls on a

*Transponder Based Aircraft Avoidance.

†The following text describes one ARGOS system, *i.e.* for one side of the LBT.

(a)

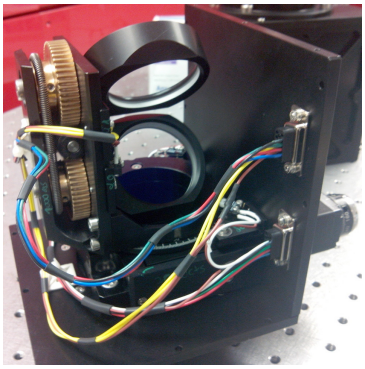

(b)

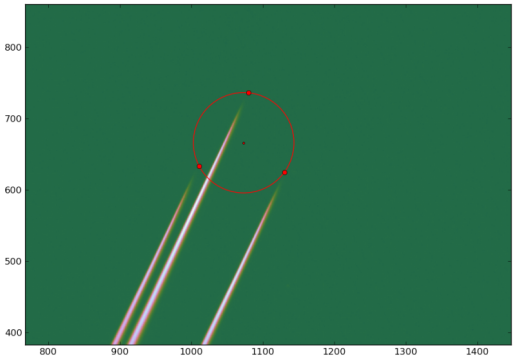

(c)

Figure 1. a) ARGOS laser constellation propagation from behind the adaptive secondary. b) Astigmatism corrector placed in the divergent beam right on top of the laser system box. c) The laser traces observed by the laser acquisition telescope One can see the tip of the cone indicated by the red circle which also identify the target position of the three lasers.

common pupil mirror that allows fine steering of the constellation on-sky and vibration compensation. The laser launch system that comes after is a refractive beam expander system consisting of a focus stage and – approximately 8 meters above – of a 40cm clear aperture singlet lens near the top of the telescope. The beam expander is followed by two large borosilicate honeycomb mirrors that directs the beams onto the sky from behind the secondary mirror. This last step is shown in Figure 1 a).

To perform the laser acquisition onto the laser wavefront sensor, we have developed[‡] recently a laser acquisition telescope presenting minimum flexure and providing a field of $\sim 1^\circ$. We are currently developing a fully automatic procedure based on the laser traces on sky (see Figure 1c). This will acquire the laser beams onto the patrol camera of the LGS wavefront sensor (described below) by controlling the launch mirror positions.

While the individual laser heads have shown a stable behavior, one of the main issue is the temperature-dependent bending of the two flat mirrors of the launch system impacting the laser spot quality. This introduces mainly defocus and astigmatism that depends on the deposited laser power (less than a watt), wind orientation, and outdoor temperature. This time-variable effect appeared problematic for proper wavefront sensing and is addressed by two means : by installing controlled heaters on the back surface of both mirrors which can stabilize the temperature gradient between front and back surfaces; and by introducing two tilted plane parallel plates in the diverging beam in the beam expander path. The latter, shown in Figure 1b, enables us to introduce variable astigmatism (and focus) in function of the tilt angle of the plates, *i.e.* up to ~ 0.9 astigmatism wave rms[§]. The

[‡]the previously used camera showed a few weaknesses such as relative high flexure, smaller field of view, and old detector. It also did not allow us to develop an automatic acquisition routine.

[§]the limited range of introduced astigmatism is usually insufficient during the laser propagation thus requiring the heater on the back surfaces as mentionned above.

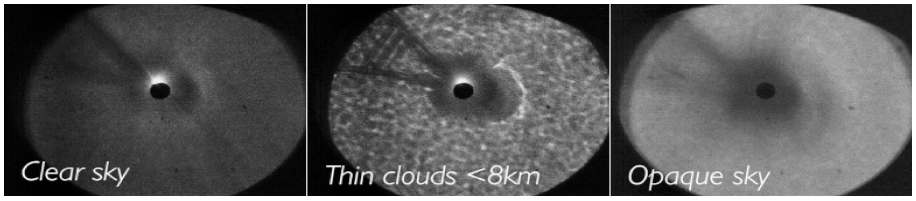

Figure 2. Patrol camera images in different cloud conditions. The patrol cameras allow the fine acquisition (FoV is $\sim 1'$) and guiding of the LGS. The central black circle is actually the individual field stop, $\sim 4.5''$ wide, of the wavefront sensor. Opacity and clouds altitude have different effect on the return flux and our ability to sense the atmospheric turbulence.

subsequent spot optimization (see also 15 in this proceeding) is still in development and a final characterization of the stability and the residual effects on-sky is still pending.

LGS Wavefront Sensing Along the propagation paths, some photons are scattered by air molecules, and after 80μs those from 12km distance arrive back to the telescope. After the tertiary mirror, a dichroic system (*i.e.* dichroic plus mirror) in front of LUCI directs the laser light towards the LGS wavefront sensor. Inside the sensor, the light from 12km is collimated. Those individual collimators also provide the capability to recenter each pupil.[15,16] The following PZT[¶] mirrors compensate each LGS jitter at 1kHz. The properly controlled beams are then directed towards the Pockels cell gating units that slice out all photons that are not being scattered at 12km $\pm$ 75m. After some additional relay optics, the wavefront is sampled by a lenslet array finally focussing the light onto the PNCCD detector. Laser firing and Pockels cells (80μs later) triggers are synchronized at 10kHz, where the PNCCD detector[17,18] is typically read at 1kHz.

The analog signal of the detector goes to the ARGOS real-time computational unit (also called BCU) which acts as a framegrabber, slope computer, piezo controller for the jitter stabilization loops, and collector of the slopes from the APD tip-tilt sensor and from the First Light Adaptive Optics (FLAO) pyramid wavefront sensor (e.g., 19). So the ARGOS BCU is literally at the nerve center of the real time stream which is also described in more details in 15. The set of tip-tilt and wavefront measurements is finally sent to the adaptive secondary real-time computer for AO control.

During the commissioning of this sub-system and the Pockels cell in high altitude, an unforeseen effect was the ozone production caused by the high voltage required by the units. The produced ozone corroded non-metallic elements, destroying the mechanical alignement of the unit which resulted in very poor suppression rate of the "Rayleigh column". After a complete revision of the opto-mechanical and power supply designs, we now have much more robust Pockels cells providing consistent high suppression rate of >3000 (open to close shutter ratio).

The acquisition of the lasers onto the sensor is performed by dedicated cameras. These LGS patrol cameras are fed by annular mirrors placed before the first collimator lens. The inner diameter of those mirrors defines the field stop with an aperture of $\sim 4.5''$. While the whole assembly is very useful to fine-acquire and guide the lasers on the WFS based on the patrol camera images (see Figure 2), admittedly this represents also one weakness of the design. Indeed, because the field stop is before the jitter compensation mirror, too high vibrations can potentially drive the light out of the sensor. This put strong requirements on our jitter, flexure and vibration algorithms and hardwares (e.g. accuracy of the launch mirror).

In clear-sky condition, the return flux measured on the WFS detector is as expected : approximately 900 photons/subaperture/milli-second for 1μs opening time per laser pulse, with 8×8 pixels per subapertures and 15 subapertures along the pupil diameter. This large flux offers us an ample margin in term of return flux conditions, *i.e.* 5 to 10 times more. It can be much needed as the number of photons can be greatly reduced when thin clouds are present, depending on their altitudes and obviously their opacities. This is illustrated in Figure 2 with images acquired by one patrol camera of the LGS WFS. From our current understanding, the large laser power – to allow a minimum return flux from 12km$\pm$75m – and high Pockels cell suppression rates – to suppress effectively the enhanced returned flux from undesired altitude – are mandatory to extend the operational range of ARGOS under most conditions.

[¶]piezo-electric transducer.

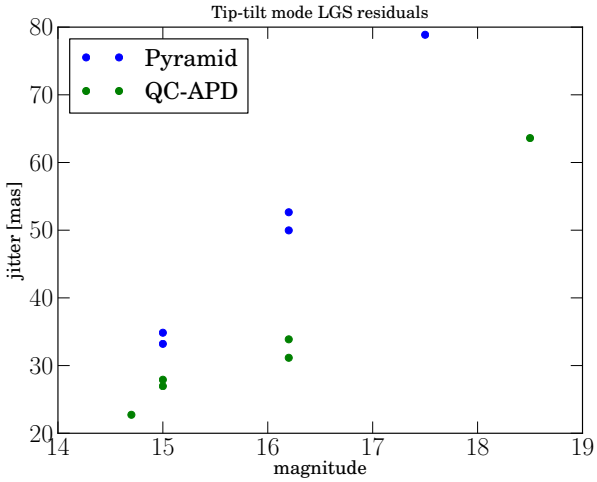

Figure 3. Comparison of the quad-cell APD with the pyramid WFS, both used as tip-tilt sensors. The comparison is performed in daytime with atmospheric turbulence emulated on the secondary mirror. The jitter is measured here from the LGS wavefront sensor tip-tilt residuals. While it may be an optimistic prediction with respect to nighttime condition due to low vibration level, this comparison suggests that the QC APD tip-tilt sensor brings an improvement of more than a magnitude with respect to the pyramid.

Tip-Tilt Wavefront Sensing and Truth Sensing In addition to the LGS wavefront sensor, ARGOS has implemented a quad-cell avalanche photodiode (QC APD) tip-tilt sensor running at up to 1kHz. It is integrated to the FLAO pyramid WFS board that sits in the LUCI derotator in front of the instrument. This tip-tilt sensor was implemented to reach the faintest magnitude possible, thus extending the sky coverage and allowing operations in deep field where high-redshift galaxies are typically observed. The first comparison in daytime with the pyramid used as a tip-tilt sensor indicates that the ARGOS QC APD brings an improvement of at least one magnitude, suggesting a *R*-band limiting magnitude of 18.5mag and possibly fainter, see Figure 3. The faint magnitude regime with the QC APD tip-tilt sensor has to be further investigated on-sky.

Finally, non-common path aberrations (NCPA) between the LGS WFS and the FLAO pyramid WFS are measured by the pyramid. The slowly measured 20 first modes are projected on the LGS WFS and offloaded to the LGS slope offsets. This truth sensing is mandatory to obtain good image quality with ARGOS. We note however that it does not include the NCPA between the FLAO board and the LUCI detector; aberrations that are negligible in the ARGOS regime.

In practice, since both tip-tilt and pyramid are on the same optical board, the light of a single star is splitted following a selective ratio, which has been typically 50/50. This concept and assembly, while providing us with exquisite wavefront measurements, relies on the FLAO board to be fully operational. On a different topic, it also opens the possibility to perform hybrid adaptive optics, combining laser and natural guide star measurements to push towards fainter NGS in the diffraction limited regime.[20]

Daytime calibration and closed-loop The calibration strategy of ARGOS is based on daytime closed-dome operation. To simulate the on-sky off-axis LGSs and on-axis NGS, a delicate optical unit has been developed that can be placed right at the prime focus of LBT directly illuminating the adaptive secondary. The unit[21] incorporates a computer generated phase hologram that reproduces the off-axis aberrations (∼220 waves of coma and ∼70 waves of spherical aberration) normally introduced by the primary mirror. This allows us to properly calibrate our system and perform daytime atmospheric emulation, as described below.

The LGS interaction matrix acquisition and the daytime turbulence emulation follow the same concept as developed for the FLAO system. We therefore refer to 19 for more thorough explanations on some aspects of the AO system calibration and summarize here the operation relevant to ARGOS.

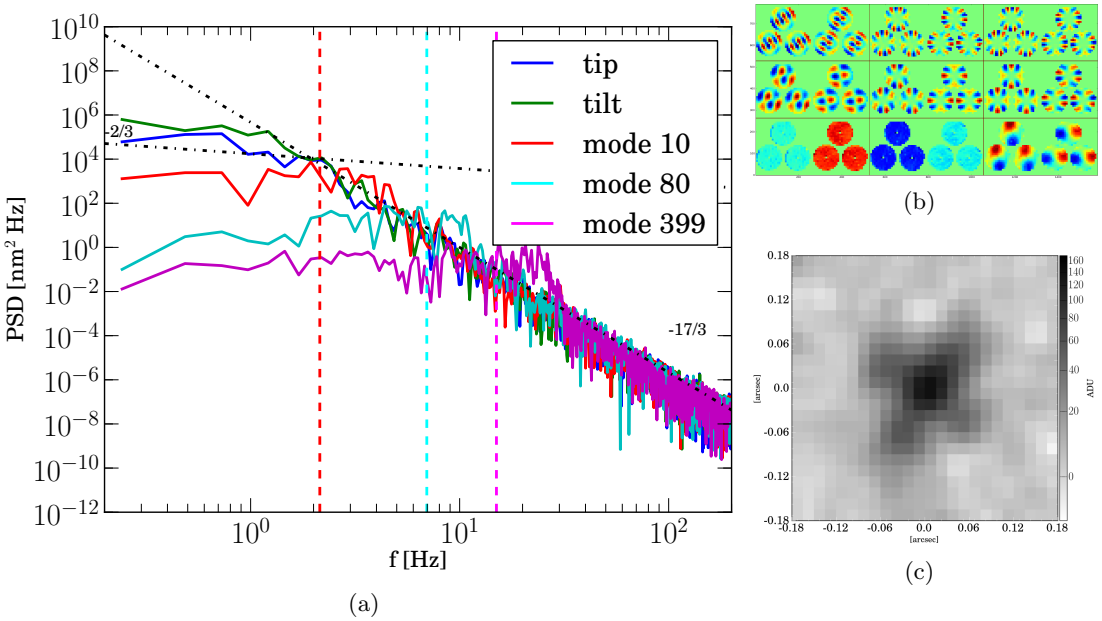

Figure 4. Illustration of the day-time operation. a) Example of temporal power spectra applied on the ASM via the disturbance vector. The simulated parameters are $V_{wind} = 15m/s$, $L_0 = 40m$, and seeing of $1.2''$. b) the x and y slopes for all three LGS obtained for nine different mode of the interaction matrix acquisition process. c) On-axis PSF on LUCI with the diffraction limited N30 camera with a pixel scale of $0.015''$/pixel. Atmospheric disturbance is emulated on the secondary mirror, the LGS loop is close on the off-axis calibration sources, tip-tilt and truth sensing on the on-axis one. See text for more comment.

The LGS modal interaction matrices (IM) are obtained by using our off-axis calibration sources illuminating the Adaptive Secondary Mirror (ASM). This is performed by a sequence of push-and-pull of a given amplitude for each of the 150 modes and by recording the WFS slopes. The amplitude is fine-tuned for each mode to avoid saturation as well as to obtain uniform signal strength on the WFSs. All three LGS interaction matrices are acquired simultaneously and thus rely on the proper alignment of all three off-axis calibration sources to the LGS WFS. The tip-tilt interaction matrix is either acquired similarly with the on-axis calibration source or by using the already calibrated pyramid wavefront sensor converting pyramid tip-tilt to QC tip-tilt.

The atmosphere emulation is introduced in the optical path by the ASM itself. This is done by defining a disturbance position vector, $c_{disturb}$, which is added to the calculated position commands of the ASM. We use this disturbance commands in a synchronous way, *i.e.* the disturbance is systematically added at each AO loop step (in practice at the sampling frequency $f_s = 1$kHz). The power spectra density of this disturbance is illustrated in Figure 4 a). Except for a slight overshoot, the resulting turbulence is in agreement with expected asymptotical power laws and presents the predicted cutoff frequencies,[22] as approximated by $f_{cut} \approx 0.3(n+1)V_{wind}/D$ with n being the Zernike radial degree. Since this atmospheric emulation is conjugated to the ground layer, the daytime operations with ARGOS are diffraction limited unlike during nighttime.

Figure 4 illustrates the typical daytime operation : from the synchronous LGS interaction matrix acquisition, to the atmospheric emulation, and finally the adaptive optics control resulting in a sharp PSF on the diffraction limited N30 LUCI camera (scale of $0.015''$/pixel). The obtained Strehl is typically of order ∼50% and is mostly dominated by the residual NCPAs between the pyramid WFS and LUCI, which in nighttime are negligible for ARGOS. The cross-pattern is qualitatively justified by the mapping of the 15×15 ARGOS subapertures to the 672 actuators: on average one subaperture sees 4 actuators[‖] which causes uncontrolled modes to appear.

Night-time Sequence The nighttime operations are naturally a bit more complex due to the necessary laser control, the vibration compensation and the higher layer uncorrected turbulence. We summarize here our closed-

[‖] on average since the actuator arrangement is not rectangular.

loop sequence on-sky and refer to 15 for more detail :

- Laser clearance and propagation.
- Laser acquisition : first, the acquisition with the large field laser acquisition telescope to bring the laser light onto the patrol camera, then the laser spot optimization (focus and astigmatism), and finally the fine acquisition from the patrol camera field of view to the LGS WFS.
- Laser guiding : after acquisition on the WFS, the guiding is started using either the patrol camera images or the jitter mirror positions to perform the appropriate offloads.
- The LGS pupil centering & the jitter compensation loops are enabled to ensure a proper conjugation to the adaptive secondary mirror and to remove the LGS tip-tilt.
- Closing the NGS tip-tilt loop with the QC APD.
- Co-centerering of the NGS on the pyramid WFS.
- Nulling of the LGS focus : this is performed to maximize the dynamical range of the WFS. We measure the LGS static focus from the LGS Shack-Hartmann, convert it to a time of flight delay of the laser beacons, and finally modify the delay between the laser pulse and the Pockels cells opening.
- Closing the higher-order loop on the LGS wavefront sensors.
- Starting the truth sensing loop of ∼20 modes with the pyramid: adjustment of the SH slope offsets and of the LGS time of flight based on the slow measurement of the first ∼20 modes on the pyramid WFS.

The full procedure takes usually approximately one minute. Following that, science exposure can start and if requested dithering or slit nodding.

3. FIRST ON-SKY RESULTS

ARGOS performed its first loop closure on all three LGS in December 2014 on the right eye of the LBT. We chose to point towards NGC2419, the so-called "Intergalactic Wanderer" at the outskirt of our galaxy, for its appropriate extent on sky and its numerous stars. Within short exposures, the distant globular cluster offered us the possibility to assess the correction gain and in particular the increased point source sensitivity. Later in May 2015, we performed hour-long integrations and repeated the good performances over several nights. During that commissionning run, the nearby barred spiral galaxy NGC6384 was observed mostly in H- and J-band for a total of more than one hour. We analyze those exposures here to study the improved PSF sizes.

Those two sets of observations allow us to discuss the major improvements brought by ARGOS : the increased sensitivity and the uniform improved resolution, *i.e.* two facets of ground-layer correction that also apply to spectroscopy.

3.1 Point source sensitivity

After data reduction and combination of the images, we perform PSF photometry on the globular cluster NGC2419 to assess the improvement in point source sensitivity. To do so we use the standard package DAOPHOT[23] in PYRAF. This software package allows us to construct a PSF model based on an analytical profile with additional quadratic variations across the FoV. This approach seems adapted to GLAO data having a well behaved PSF; and a good model can be build for the full $4' \times 4'$ FoV. Based on the constructed PSF, one can extract the photometry in crowded field by simultaneous PSF fitting. After a few iterations on the residual images, one is able to pick the faintest stars and obtain a complete catalog. The PSF modelling performed beforehand requires to select as many isolated stars as possible spread across the field : typically between 20 to 40 in our case depending on the band and the exposure time. The full process is performed on three different images : 5 minute exposure uncorrected and AO corrected, and 15 minute exposure AO corrected. The results is three star catalogs that can be easily compared.

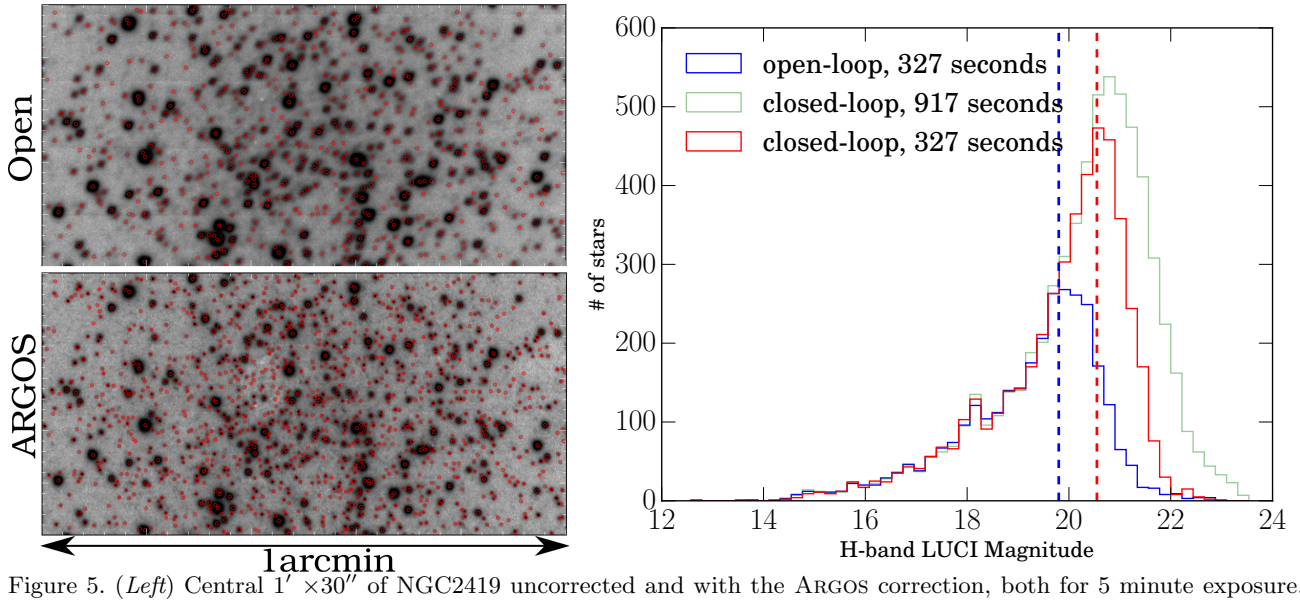

Figure 5. (*Left*) Central $1' \times 30''$ of NGC2419 uncorrected and with the ARGOS correction, both for 5 minute exposure. Square root stretched intensity scale. Overlaid in red circles are the detected stars with DAOPHOT whose photometry is used for the plot on the right side. (*Right*) Luminosity function of NGC2419 for three different images 5 minute uncorrected (blue) and with ARGOS (red), and 15 minutes with ARGOS. The vertical curves indicate the peak of the distributions of the 5 minute exposure AO corrected and uncorrected. They are separated by ∼0.75 magnitude which is inline with the expected improvement brought by ARGOS.

In Figure 5, we show open-loop and ARGOS corrected images based on 5 minute exposure for the central $1'$ $\times 30''$. Identified stars are indicated by small red circles and the luminosity functions for the full $4' \times 4'$ FoV is represented on the right of Figure 5. The vertical dashed-lines indicate the peaks of the luminosity function distributions in open and closed-loop for 5 minute exposure.

The delta magnitude, *i.e.* the improved sensitivity, between the two distribution peaks is ∼0.75 mag. This can be explained as follows. In the background limited regime, for a point source and fixed flux the signal-to-noise ratio scales as

$$\frac{\mathrm{S}}{\mathrm{N}} \propto \frac{f_{\mathrm{aper}} t_i}{\sqrt{d^2_{\mathrm{aper}} t_i}}, \tag{1}$$

where f_{aper} is the fraction of the source flux into the aperture (or slit), d_{aper} is the diameter of the aperture, and t_i is the integration time. If the PSF size is reduced by a factor 2, for a fixed fraction of the source flux f_{aper}, the diameter of the aperture can be divided by 2[**]. It results that the S/N is itself multiplied by two for a fixed integration time, equivalent to a delta of 0.75 mag. This reasoning explains partly the luminosity function in Figure 5, and in particular the sensitivity extension for a same exposure in closed-loop. Another aspect that we do not discuss here is the reduced crowding noise; noise that can be a serious limitation on the depth one can reach in dense fields.

This increased point source sensitivity is an important argument for the advantage of GLAO system. It can also be turned around : for a fixed signal-to-noise ratio one can shorten the integration time by a factor of ∼4, hence augmenting the efficiency of the observations.

Finally, this sensitivity improvement is also beneficial for spectroscopy. For a point source, one can select a narrower slit thus decreasing the background noise for a fixed source flux. Narrower slit also allows to reach higher spectroscopic resolution for a same signal-to-noise ratio, which is advantageous to reduce the contamination from the numerous atmospheric OH lines in the near-infrared. Last, AO correction also improves the slit coupling hence improving the throughput of the observations.

[**]To be more exact, one should consider the encircled energy of a given fraction f_{aper} of the flux rather than the PSF FWHM. Both are however equivalent if the PSF profile stays the same between open and closed-loops.

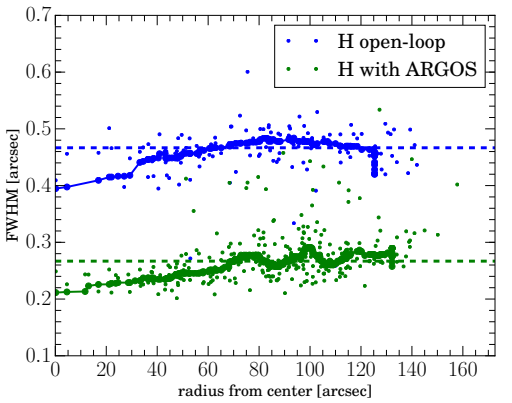

(a)

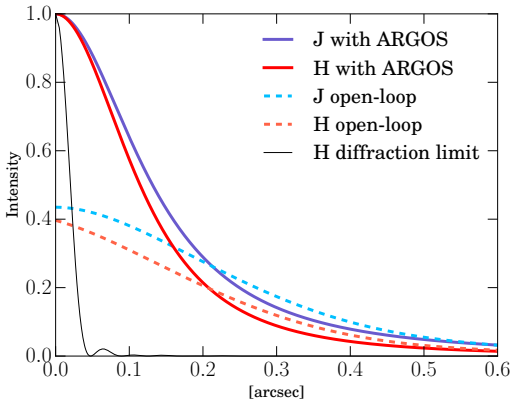

(b)

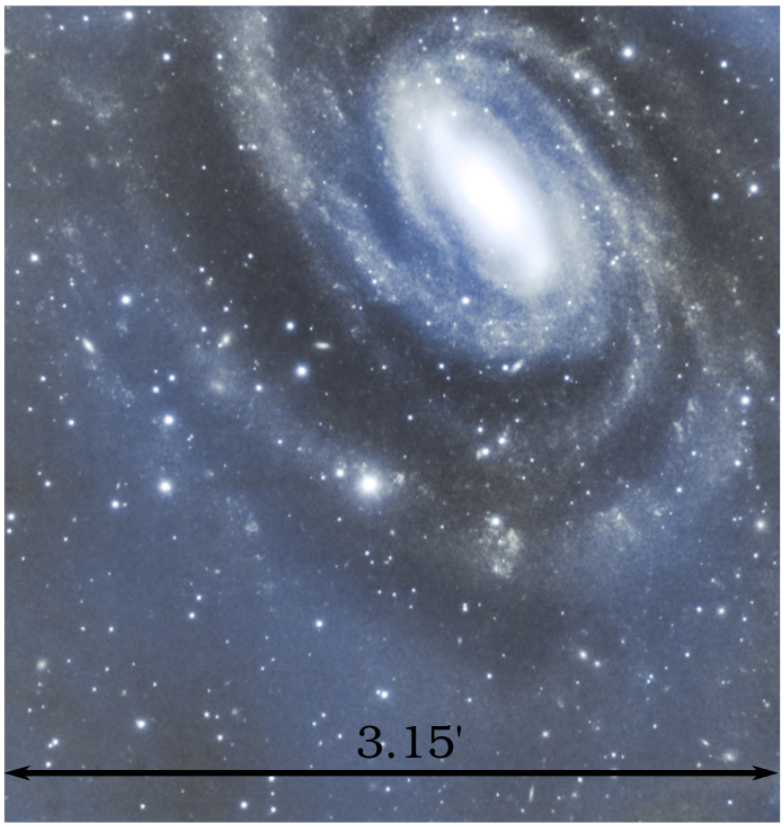

(c)

Figure 6. (a) H-band FWHM as a function of radius from the center of the field, *i.e.* from the tip-tilt star, in closed and open-loop. This is done by automatic detection and individual fit of 2D elliptical Moffats. The median, 0.27″ and 0.46″ respectively, are indicated by dashed lines. There is a small trend with radius which is however seen in both corrected and uncorrected cases. Therefore, we cannot attribute it directly to anisoplanatism of the GLAO correction. (b) PSF radial profiles of the GLAO corrected images in J- and H-band fitted on the stacked radial profile of ∼20 stars taken in the NGC6384 field of view. The J- and H- bands have FWHMs of 0.26″ and 0.23″ respectively against 0.51″ and 0.41″ when uncorrected. The uncorrected profiles are normalized by the peaks of their corrected counterparts. As a reference, the H-band diffraction limit PSF is indicated. (c) Composite image of NGC6384 based on 30 minute exposure in both J- and H-band, showing exquisite resolution over a squared ∼3.15′.

3.2 Point spread function full width at half maximum

To analyze more systematically the improvement in PSF FWHM sizes and the uniformity of the correction within the 4′×4′ FoV, we automatize the point source detection[††] and we fit 2-D elliptical Moffat profiles with varying power law index. The Moffat fits typically well the PSF both for seeing limited[24] and GLAO corrected images. These tool allows us to verify the PSF size improvement and its uniformity over the field of view. Thanks to the long integration in both J- and H-band obtained in May 2015, we emphasize here the analysis done on NGC6384.

We illustrate the results in Figure 6 a) for the H-band by plotting the FWHM as a function of radial distance from the center. We perform the same analysis in other bands for the same galaxy and on NGC2419, as shown later in Figure 7.

In a parallel analysis, we select about 20 stars in the field of view, scaled them and fit their combined radial profiles. The results is presented in Figure 6 b) where we compare J- and H-bands uncorrected and with the

[††]based on Photutils an affiliated package of Astropy, sets of python routines based themselves on IRAF.

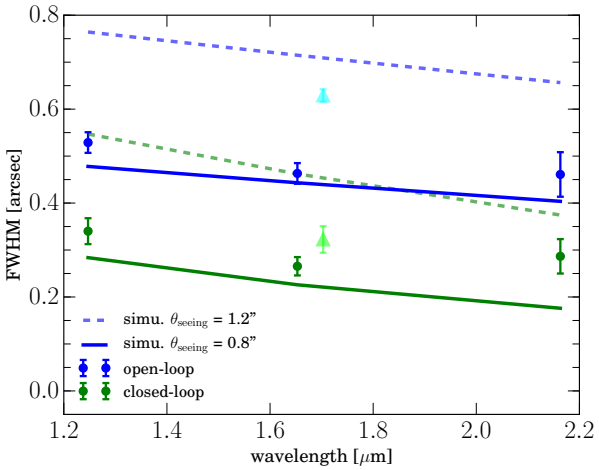

Figure 7. Comparison of early simulation with observations for the three bands : J, H, and Ks. Blue indicates uncorrected observations or simulations. Green indicates a correction with ARGOS. The dashed and plain lines represent simulation in the three broad bands with outer layer $L_0 = 30$m and seeing of $1.2''$ and $0.8''$ respectively. Data are based on observations from December 2014 and May 2015, with exposure time from <1 minute (K-band) to 15 - 30 minutes. Seeing measured by the DIMM at LBT was between $0.8''$ to $1.2''$.

ARGOS correction. The uncorrected PSF are normalized by the same factor than their respective AO corrected bands, highlighting the enhanced encircled energy at small radii.

The main conclusion is that we achieve here a reduction factor of > 1.5 in PSF size and that no anisoplanatism is detectable.

Finally, in Figure 7, we compare our observations from December 2014 and May 2015 with early simulations. We plot the PSF FWHM size for J- H- and Ks-band as measured from open and closed-loop data; the seeings measured by the DIMM were typically between $0.8''$ to $1.2''$. We compare those observations to simulation of $1.2''$ and $0.8''$ seeing and an outer layer of $L_0 = 30m$. Those are represented by the plain and dashed curves respectively, open-loop is represented in blue and closed-loop in green. This comparison illustrates the good agreement of our on-sky observations to the expected performances.

4. CONCLUSION

As the commissioning proceed and we gain experience with ARGOS, we have the opportunity to gather more information and answer some questions relevant to ELTs : how is the atmospheric ground-layer varying in time, and with the seasons? which fraction of the distortion can be corrected? which spot elongation can be tolerated? what is the impact of the tip-tilt magnitude and its position in the field? and which sky coverage can be achieved with a 8m-class telescope? How does the PSF change in time? Or more generally, what are the key ingredients for a robust ground layer adaptive optics system on a large telescope?

In the current state, we have shown here that ARGOS is reaching its expected performances on-sky, *i.e.* an improvement of a factor of about 2 in FWHM over the $4' \times 4'$ FoV. After the first ARGOS loop closure in December 2014, we have performed a long exposure observation of NGC6384 for a total of one hour in J and H-band. The high resolution image, $\sim 0.3''$ PSF FWHM, over the full field of view is illustrated in Figure 6 c). Following those milestones, we look forward to a full scientific demonstration of the joined LUCI and ARGOS facility.

At the time of writing, we have started to commission the ARGOS left side and we have demonstrated similarly good performances. We have progressed on observational procedures and the interaction between LUCI and ARGOS, implementing full observing sequences including dithering. And while many operational aspects concerning mostly software development have still to be finalized, ARGOS is getting close to reach one of its main goals : to carry efficiently long exposure observations taking full benefit of the multiplexing possibility, the

improved sensitivity for point-like object, and to perform spatially resolved slit spectroscopy.

ACKNOWLEDGMENTS

This research has made use of NASA's Astrophysics Data System Bibliographic Services, of Astropy, a community-developed core Python package for Astronomy,[25] and of DAOPHOT.[23]

REFERENCES

[1] Rigaut, F., "Ground Conjugate Wide Field Adaptive Optics for the ELTs," in [*European Southern Observatory Conference and Workshop Proceedings*], Vernet, E., Ragazzoni, R., Esposito, S., and Hubin, N., eds., *European Southern Observatory Conference and Workshop Proceedings* **58**, 11 (2002).

[2] Tokovinin, A., Baumont, S., and Vasquez, J., "Statistics of turbulence profile at Cerro Tololo," MNRAS **340**, 52–58 (Mar. 2003).

[3] Egner, S. E., Masciadri, E., and McKenna, D., "Generalized SCIDAR Measurements at Mount Graham," PASP **119**, 669–686 (June 2007).

[4] Buschkamp, P., Seifert, W., Polsterer, K., Hofmann, R., Gemperlein, H., Lederer, R., Lehmitz, M., Naranjo, V., Ageorges, N., Kurk, J., Eisenhauer, F., Rabien, S., Honsberg, M., and Genzel, R., "LUCI in the sky: performance and lessons learned in the first two years of near-infrared multi-object spectroscopy at the LBT," in [*Society of Photo-Optical Instrumentation Engineers (SPIE) Conference Series*], *Society of Photo-Optical Instrumentation Engineers (SPIE) Conference Series* **8446**, 84465L (Sept. 2012).

[5] Dressel, L., [*Wide Field Camera 3 Instrument Handbook, Version 7.0*] (2015).

[6] Birkmann, S. M., Ferruit, P., Alves de Oliveira, C., Böker, T., De Marchi, G., Giardino, G., Sirianni, M., Stuhlinger, M., Jensen, P., Rumler, P., Falcolini, M., te Plate, M. B. J., Cresci, G., Dorner, B., Ehrenwinkler, R., Gnata, X., and Wettemann, T., "Status of the JWST/NIRSpec instrument," in [*Society of Photo-Optical Instrumentation Engineers (SPIE) Conference Series*], *Society of Photo-Optical Instrumentation Engineers (SPIE) Conference Series* **9143**, 914308 (Aug. 2014).

[7] Marchetti, E., Hubin, N. N., Fedrigo, E., Brynnel, J., Delabre, B., Donaldson, R., Franza, F., Conan, R., Le Louarn, M., Cavadore, C., Balestra, A., Baade, D., Lizon, J.-L., Gilmozzi, R., Monnet, G. J., Ragazzoni, R., Arcidiacono, C., Baruffolo, A., Diolaiti, E., Farinato, J., Vernet-Viard, E., Butler, D. J., Hippler, S., and Amorin, A., "MAD the ESO multi-conjugate adaptive optics demonstrator," in [*Adaptive Optical System Technologies II*], Wizinowich, P. L. and Bonaccini, D., eds., *Society of Photo-Optical Instrumentation Engineers (SPIE) Conference Series* **4839**, 317–328 (Feb. 2003).

[8] Hart, M., Milton, N. M., Baranec, C., Powell, K., Stalcup, T., McCarthy, D., Kulesa, C., and Bendek, E., "A ground-layer adaptive optics system with multiple laser guide stars," Nature **466**, 727–729 (Aug. 2010).

[9] Tokovinin, A., Tighe, R., Schurter, P., Cantarutti, R., van der Bliek, N., Martinez, M., Mondaca, E., and Heathcote, S., "Performance of the SOAR adaptive module with UV Rayleigh guide star," in [*Society of Photo-Optical Instrumentation Engineers (SPIE) Conference Series*], *Society of Photo-Optical Instrumentation Engineers (SPIE) Conference Series* **8447**, 4 (July 2012).

[10] Rabien, S., Barl, L., Beckmann, U., Bonaglia, M., Borelli, J. L., Brynnel, J., Buschkamp, P., Busoni, L., Christou, J., Connot, C., Davies, R., Deysenroth, M., Esposito, S., Gässler, W., Gemperlein, H., Hart, M., Kulas, M., Lefebvre, M., Lehmitz, M., Mazzoni, T., Nussbaum, E., Orban de Xivry, G., Peter, D., Quirrenbach, A., Raab, W., Rahmer, G., Storm, J., and Ziegleder, J., "Status of the ARGOS project," in [*Society of Photo-Optical Instrumentation Engineers (SPIE) Conference Series*], *Society of Photo-Optical Instrumentation Engineers (SPIE) Conference Series* **9148**, 1 (July 2014).

[11] Orban de Xivry, G., Bonaglia, M., Borelli, J., Busoni, L., Connot, C., Esposito, S., Gaessler, W., Kulas, M., Mazzoni, T., Puglisi, A., Rabien, S., Storm, J., and Ziegleder, J., "ARGOS wavefront sensing: from detection to correction," in [*Society of Photo-Optical Instrumentation Engineers (SPIE) Conference Series*], *Society of Photo-Optical Instrumentation Engineers (SPIE) Conference Series* **9148**, 34 (Aug. 2014).

[12] Bonaglia, M., Busoni, L., Mazzoni, T., Puglisi, A., Antichi, J., Esposito, S., Orban de Xivry, G., and Rabien, S., "Pre-shipment test of the ARGOS laser guide star wavefront sensor," in [*Society of Photo-Optical Instrumentation Engineers (SPIE) Conference Series*], *Society of Photo-Optical Instrumentation Engineers (SPIE) Conference Series* **9148**, 5 (Aug. 2014).

[13] Kulas, M., Borelli, J. L., Gässler, W., Peter, D., Rabien, S., Orban de Xivry, G., Busoni, L., Bonaglia, M., Mazzoni, T., and Rahmer, G., "Practical experience with test-driven development during commissioning of the multi-star AO system ARGOS," in [*Society of Photo-Optical Instrumentation Engineers (SPIE) Conference Series*], *Society of Photo-Optical Instrumentation Engineers (SPIE) Conference Series* **9152**, 0 (July 2014).

[14] Coles, W. A., Murphy, T. W., Melser, J. F., Tu, J. K., White, G. A., Kassabian, K. H., Bales, K., and Baumgartner, B. B., "A Radio System for Avoiding Illuminating Aircraft with a Laser Beam," PASP **124**, 42–50 (Jan. 2012).

[15] Busoni, L. and et al., "Commissioning of ARGOS at LBT : LGS acquisition and AO procedures," in [*in this proceeding*], (2015).

[16] Busoni, L., Bonaglia, M., Carbonaro, L., Mazzoni, T., Antichi, J., Esposito, S., Orban De Xivry, G., and Rabien, S., "Integration and laboratory characterization of the ARGOS laser guide star wavefront sensors," in [*Proceedings of the Third AO4ELT Conference*], Esposito, S. and Fini, L., eds., 92 (Dec. 2013).

[17] Orban de Xivry, G., Rabien, S., Barl, L., Esposito, S., Gaessler, W., Hart, M., Deysenroth, M., Gemperlein, H., Strüder, L., and Ziegleder, J., "Wide-field AO correction: the large wavefront sensor detector of ARGOS," in [*Society of Photo-Optical Instrumentation Engineers (SPIE) Conference Series*], *Society of Photo-Optical Instrumentation Engineers (SPIE) Conference Series* **7736**, 5 (July 2010).

[18] Orban de Xivry, G., Ihle, S., Ziegleder, J., Barl, L., Hartmann, R., Rabien, S., Soltau, H., and Strueder, L., "The ARGOS wavefront sensor pnCCD camera for an ELT: characteristics, limitations and applications," in [*Proceedings of the Second AO4ELT Conference*], (2011).

[19] Esposito, S., Riccardi, A., Quirós-Pacheco, F., Pinna, E., Puglisi, A., Xompero, M., Briguglio, R., Busoni, L., Fini, L., Stefanini, P., Brusa, G., Tozzi, A., Ranfagni, P., Pieralli, F., Guerra, J. C., Arcidiacono, C., and Salinari, P., "Laboratory characterization and performance of the high-order adaptive optics system for the Large Binocular Telescope," Appl.Optics **49**, G174 (Nov. 2010).

[20] Bonaglia, M., Busoni, L., Quirós-Pacheco, F., and Esposito, S., "Diffraction limited operation with ARGOS: a hybrid AO system," in [*Society of Photo-Optical Instrumentation Engineers (SPIE) Conference Series*], *Society of Photo-Optical Instrumentation Engineers (SPIE) Conference Series* **7736**, 77362W (July 2010).

[21] Schwab, C. and Rakich, A., "Rayleigh laser guide star calibration unit for the Large Binocular Telescope," Appl.Optics **49**, G53 (June 2010).

[22] Conan, J.-M., Rousset, G., and Madec, P.-Y., "Wave-front temporal spectra in high-resolution imaging through turbulence.," *Journal of the Optical Society of America A* **12**, 1559–1570 (July 1995).

[23] Stetson, P. B., "DAOPHOT - A computer program for crowded-field stellar photometry," PASP **99**, 191–222 (Mar. 1987).

[24] Trujillo, I., Aguerri, J. A. L., Cepa, J., and Gutiérrez, C. M., "The effects of seeing on Sérsic profiles - II. The Moffat PSF," MNRAS **328**, 977–985 (Dec. 2001).

[25] Astropy Collaboration, Robitaille, T. P., Tollerud, E. J., Greenfield, P., Droettboom, M., Bray, E., Aldcroft, T., Davis, M., Ginsburg, A., Price-Whelan, A. M., Kerzendorf, W. E., Conley, A., Crighton, N., Barbary, K., Muna, D., Ferguson, H., Grollier, F., Parikh, M. M., Nair, P. H., Unther, H. M., Deil, C., Woillez, J., Conseil, S., Kramer, R., Turner, J. E. H., Singer, L., Fox, R., Weaver, B. A., Zabalza, V., Edwards, Z. I., Azalee Bostroem, K., Burke, D. J., Casey, A. R., Crawford, S. M., Dencheva, N., Ely, J., Jenness, T., Labrie, K., Lim, P. L., Pierfederici, F., Pontzen, A., Ptak, A., Refsdal, B., Servillat, M., and Streicher, O., "Astropy: A community Python package for astronomy," A&A **558**, A33 (Oct. 2013).